A study on hydrodynamics of melt expulsion in pulsed Nd: YAG laser drilling of titanium

Shashank Sharma*[1], Yash Pachaury[2], Syed Nadeem Akhtar[3], J.Ramkumar[1]
[1]Indian Institute of Technology Kanpur
[2]Indian Institute of Information Technology Design and Manufacturing Jabalpur
[3]Integral University Lucknow
*Corresponding author: NL-115, Dept. of Mechanical Engineering, IITK, Kanpur-208016, kshashan@iitk.ac.in

Abstract: Laser drilling of titanium and its alloys is widely used in aerospace industry, as it offers selective removal of material at high accuracy and speed. However, laser drilling often inherits defects such as large heat affected zone, micro cracks and recast layer. These defects depend upon complex melting and solidification phenomena happening due to interaction of high intensity laser with the material.

Therefore, to understand and control these processes, a multi-phase (solid, liquid, and vapor) axisymmetric model is computed using Comsol Multiphysics(R). Moving mesh feature is used to simulate the melt displacement based on the physical processes involved. The model also studies the effect of different laser intensity profiles (ideal gaussian profile (TEM_{00}) and a top-hat profile) on temperature distribution, melt velocity and the shape of the keyhole. The study is useful in optimizing the laser parameters to obtain features with minimum re-solidification, which in turn affect the surface roughness of the ablated region.

Keywords: Nd:YAG Laser drilling, melt expulsion, marangoni effect, recoil pressure, keyhole.

1. Introduction

The evolution of sophisticated materials for engineering applications has posed challenges for the researchers in the domain of manufacturing to develop effective processes to realize the fabrication of components from these materials. These materials such as Ti6Al4V can be very useful in different industries owing to their high strength to weight ratio, excellent corrosive resistance and compatibility with composite structures [1], but these properties have made the fabrication of products from the raw material very difficult with conventional machining processes.

Laser machining is one such process which has overcome the aforementioned impediments, in that the surface of a material is irradiated with a high intensity laser beam which increases the temperature of the material beyond its melting point and sometimes even beyond its boiling point. Due to very large gradients of temperature at the surface of the material, flow of molten metal occurs within the melt pool which can be attributed to Marangoni convection. When the surface of the material is heated beyond its boiling temperature, a portion of vapor phase condenses after interacting with the surrounding medium and exerts a back pressure on the vapor melt interface. This back pressure is also known as recoil pressure, which splashes the molten liquid outside of the irradiated zone. The aforementioned processes produce a keyhole shaped crater, and the splashed out molten metal after cooling adheres around the keyhole forming a re-solidified edge.

There have been numerous studies on computational modeling of laser machining processes. Several researchers have contributed significantly to the evolution of this field using their analytical as well as numerical models. Bruyere et al. [2] studied the evolution of the melted zone shape and the porosity formation using a numerical model. The model used phase field approach to model the gas trapped into the welding pool and hence provided an effective way for modeling the porosities. The numerical results were validated with experimental outcomes and a harmony was found between the two. However, the modeling was done for a single pulse. Zhang et al. [3] developed a 2D model of long pulsed laser drilling on Aluminum. Phase change (melting and vaporization) was implemented into the model and the evolution of the liquid vapor interface was tracked using a modified level set method which added extra source term for evaporation and boiling effect. The influence of laser fluence and pulse duration were determined and the model was validated against the study of the laser parameters conducted experimentally. Zhang et al. [4] analyzed the formation of elongated keyhole using experimental as well as numerical simulation technique. The flow characteristics of the vapor and the molten metal within the keyhole were studied. The observations were made on a transparent material GG17 glass using a CO_2 laser beam and the finite element simulations were carried out in ANSYS.

There have been several models which take into account the effect of assisting gases for laser drilling of materials. Low et al. [5] brought the effect of the assisting gases by adding two power terms for convective cooling and exothermic reactions between the assist gases and the molten pool. This was extended by Ng et al. [6] by coupling the vapor pressure with the rate of vapor flow through the drilled hole. After reviewing through the literature articles, it became evident that the need for the development of a comprehensive numerical simulation model for laser drilling in difficult to cut materials in COMSOL is still required.

In the present article, an attempt has been made to evolve the numerical model of laser drilling process. The modeling has been carried out for titanium alloy Ti6Al4V using temperature dependent material properties. Heat flux is applied at the top surface using different optical profiles to determine the temperature distribution. The results of the heat transfer analysis are coupled with the fluid flow equations to determine the flow velocities within the melt pool. These flow velocities served as an input to the moving mesh feature of COMSOL to determine the final keyhole profile generated using the laser beam. The analysis has been carried out for single pulses as well as multiple pulses. Phase field methodology has been utilized to track the solid-liquid interface. The results of the model would serve to optimize the laser machining parameters to obtain features with minimum re-solidification. Hence, an effective methodology is developed in the present paper to minimize the surface roughness and recast layer formation over the machined specimen.

2. Mathematical Model

In order to evaluate the levels of temperature reached in the process and to obtain characteristics of melt pool, conservation of energy (heat), mass (continuity) and momentum (Navier-Stokes) equations are solved.

$$\frac{\partial \rho}{\partial t} + \nabla.(\rho u) = 0 \qquad (1)$$

$$\rho \frac{\partial u}{\partial t} + \rho(u.\nabla)\mathrm{u} = \nabla.\left[-\mathrm{pI} + \mu\left(\overrightarrow{\nabla \mathrm{u}} + \left(\overrightarrow{\nabla \mathrm{u}}\right)^{\mathrm{T}}\right)\right] - \rho\left(1 - \beta(\mathrm{T} - \mathrm{T_m})\right)\vec{\mathrm{g}} + \vec{\mathrm{F}} \qquad (2)$$

$$\rho C_p \frac{\partial T}{\partial t} + \rho C_p u \nabla T = \nabla.(k \nabla T) \qquad (3)$$

Where, ρ is density of the material (kg/m^3), p is the pressure (N/m^2), u is the molten metal velocity (m/s), C_p is the specific heat of the material (J/kgK), F is the body force (N), μ is the dynamic viscosity (Pa-s), k is thermal conductivity (W/mK), β is thermal expansion coefficient (1/K), T_m is melting temperature, I is identity matrix, g is the gravity acceleration and T is the absolute temperature (K).

In Equation 3, instead of using a source term to define the laser intensity a separate boundary heat flux is added to the heat transfer module. At the top and side boundary convection boundary condition (Eq. 4) is used, further at top boundary radiation (Eq. 5) due to high intensity laser spot is also considered, the bottom boundary is assumed to be insulated.

$$-k\frac{\partial T}{\partial y} = h[T - T_a] \quad (4)$$

$$-k\frac{\partial T}{\partial y} = h[T - T_a] - \varepsilon\sigma\left[T^4 - {T_a}^4\right] \qquad (5)$$

Moreover, Marangoni convection was also applied at the top surface using a weak constraint, eq. 6, where γ is the temperature derivative of surface tension.

$$-\mu\frac{\partial u}{\partial x} = \frac{\partial T}{\partial y}\frac{\partial \gamma}{\partial T} \qquad (6)$$

All the thermo-physical parameters (Table 1) stated in equations 1-6 are temperature dependent.

2.1 Laser parameters

When a laser light propagates through an absorbing medium it starts to attenuate and the energy contained by the photon is transferred to the colliding surface.

However, the energy transfer depends upon several factors such as laser wavelength, absorption coefficient of material, and pulse width of the laser. The pulse width dictates the mode of energy transfer, generally industrial laser used for drilling purpose operates in µs-ms pulse width range, in which primary mode of energy transfer is thermal [7] in nature. In our study, a millisecond pulsed laser is used as a heat source. Moreover, the optical penetration depth corresponding to YAG laser is very small compared to thickness of the domain (work-piece thickness) thus it would be most appropriate to incorporate the laser intensity as a boundary heat source.

In this model, both gaussian beam profile and top hat profile is used to define the laser intensity distribution spatially (Figure 1), time distribution of laser intensity is assumed to have constant rise and decay (pulse on/off) and is defined by a gaussian profile. The laser intensity used in the simulation is 2.5×10^{8} W/m^2, the beam diameter is 1.8 mm.

$$Q = I(r,t) \times \alpha \times (1-\lambda) \quad (7)$$

$$I(r,t) = \mathrm{F} \times f_{r,t} \quad (8)$$

The Equation (7) represents the boundary heat source (W/m^2), where α is the absorption coefficient of titanium for 1064nm wavelength, and λ is the reflectance of the material. In Equation (8), F is the laser fluence and the function $f_{r,t}$ is used to define a gaussian or top hat pulse train using analytical functions in comsol multiphysics.

3. Numerical Aspects

As discussed above three different phases coexist together in laser drilling process. Heat transfer with phase change module is used to keep track of these different phases. To obtain uniform transition zone, the temperature transition interval is optimized using different ∇T $(10K, 25K, and\ 50K)$.

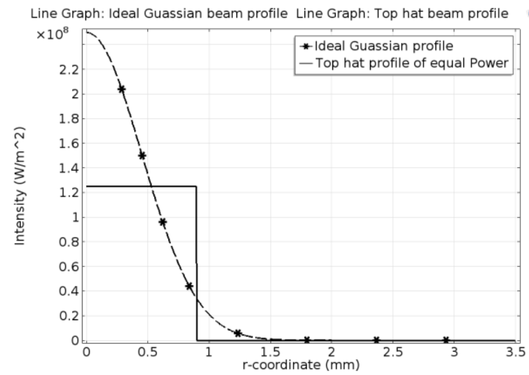

Figure 1. Laser intensity vs. radial distance. Peak intensity of gaussian beam is 2.5×10^{8}, Uniform top hat beam profile having intensity 1.25×10^{8}.

Moreover, the molten metal is considered to be laminar and the dynamic viscosity of solid is assumed to be very high i.e. 100 Pa.s. Before vaporization only surface tension and gravity forces acts on the molten metal, the effects of surface tension is implemented by using a weak constraint term on the top boundary which is dependent on tangential velocity of the melt. Further, as vaporization temperature is reached a recoil pressure acts on the vapor liquid interface whose expression [8] is given by

$$R_p = 0.54 * P_a * \exp\left(\frac{L_v(T-T_v)}{RTT_v}\right) * f_r \quad (9)$$

Where P_a atmospheric pressure L_v is latent heat of vaporization T_v is vaporization temperature and R is universal gas constant. f_r, is the spatial distribution of laser intensity which makes sure that the recoil pressure acts inside the irradiated area instead of whole boundary. The recoil pressure is exerted using an open boundary condition also the recoil pressure is effective only on those regions where temperature has reached its vaporization point.

Thus after vaporization recoil pressure will be active, and it will exert a normal downward force on the vapor liquid interface, which will result in the formation of a cavity. For modeling the cavity formation, moving mesh feature is used in which after each time step, the temperature and velocity distribution is calculated using heat transfer and laminar flow module, and the normal component of velocity is used as mesh velocity of the top boundary. Further, the domain is subjected to repetitive pulse heating meaning at every time step the domain will reach vaporization temperature, due to which certain amount of deformation will occur, and after each deformation the mesh quality will deteriorate.

A uniform triangular mesh with minimum element size of 0.8 µm is generated for the whole domain. Further for modeling of cavity formation, automatic re-meshing is used. The stop condition for automatic re-meshing are mesh quality and peak temperature, meaning whenever the peak temperature goes beyond the vaporization point deformation will occur due to recoil pressure. Thus whenever deformation happens, a newer mesh will be generated for the deformed geometry. The pulse train used for heating operates in the time interval of 2s, with pulse on and off time of 50 ms.

4. Results and Discussion

When a millisecond laser interacts with the irradiated material, the energy of photon is used to excite the lattice which in turn increases the temperature of the surface. At the initial stages of interaction only melting will occur, and the flow of melt will be dictated by the gravity and surface tension forces, in case of molten titanium the surface tension forces tends to extend the molten pool radially outward, which results in marangoni convection. Figure 2 shows the axisymmetric view of melting stage where the velocity pattern is radially outwards. It is pertinent to note that the effect of marangoni convection does not affect the drilling process primarily as latter involves vaporization.

Generally, pulsed laser is used for drilling operations which include repetitive heating and cooling of the work surface. When laser pulse is on, its intensity rises with time resulting in melting and vaporization which eventually leads to keyhole formation inside which flow of molten metal occurs. In Figure 3 (right), it can be observed that due to intense vaporization recoil pressure is acting on the interface resulting in outward flow of liquid metal and a hump of molten metal is accumulated near the edge of the keyhole. However, when cooling occur the recoil pressure decays and the gravity and surface tension force acts as the pivotal source for convection. In Figure 3 (left), it can be observed that the velocity pattern is towards the centre of the keyhole, however this type of convection generates perturbation inside the keyhole, as the retracting melt solidifies and adheres to the inside wall of the cavity.

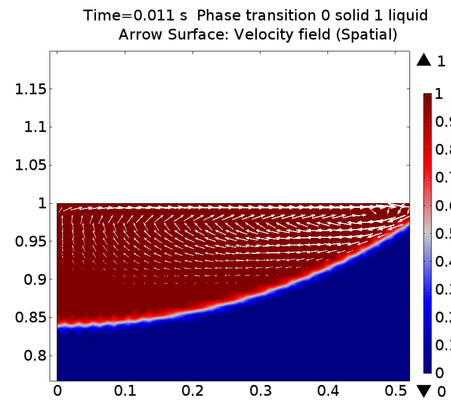

Figure 2. Melt flow due to marangoni convection at initial stage of laser material interaction.

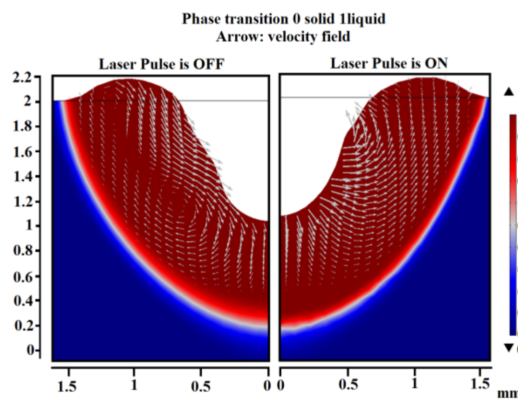

Figure 3. Phase distribution and spatial velocity field (Left: when laser pulse is OFF cooling occurs and only marangoni convection and gravitational force is effective, Right: When laser pulse is ON recoil pressure acts and splashes the molten metal as shown by the arrow plot.)

Figure 4, shows the temperature distribution and the shape of cavity when gaussian laser intensity is used. As shown in Figure 1, the laser intensity is highest at the center in case of gaussian beam which results in non uniform shape of cavity (similar to keyhole), having maximum depth at the center. It is pertinent to note that after formation of keyhole, when subsequent splashing of molten metal occurs due to further vaporization of material the splashed melt will be unable to come out of the keyhole due to its tapered nature and will adhere to the inside walls after solidification resulting in poor finish. Because of the aforementioned reasons, gaussian laser beam profile is less efficient towards drilling of uniform size holes.

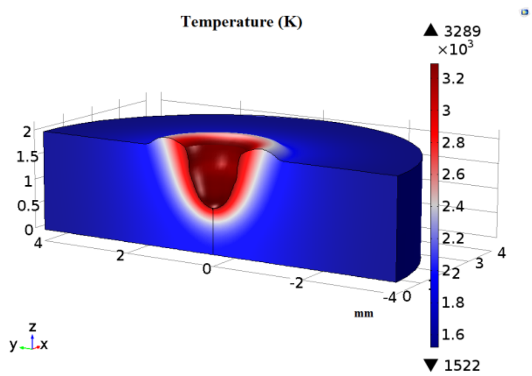

Figure 4. 3D-Temperature distribution and shape of keyhole for gaussian intensity, as the gaussian intensity have peak at its center the keyhole depth is maximum at center.

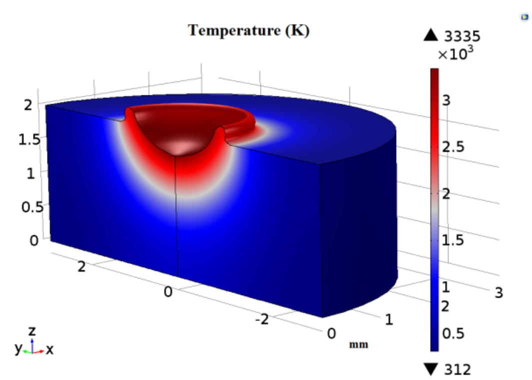

Figure 5. 3D-Temperature distribution and shape of keyhole for top hat intensity, because of uniform intensity the variation of cavity depth is very little as radial distance increases.

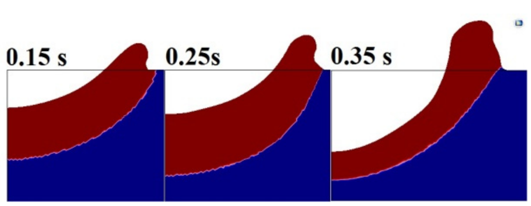

Figure 6. Evolution of the geometry of the cavity formed when a top hat laser intensity profile is used. It indicates that the size of pile up molten metal near the edge of cavity increases with increase in irradiation time.

However, when a top hat laser beam profile is used the tapered nature of the cavity is obviated. Figure 5 shows the temperature distribution of the cavity and the uniform nature of the cavity formed. However, due to uniform geometry of the cavity there is no obstruction for splashing molten metal and the size of molten hump near the edge of the cavity is more in the case of top hat laser intensity. Figure 6 shows the evolution the cavity which depicts that with time the size of accumulated molten metal near the edge of cavity will increase.

5. Conclusions

In the present study, a comprehensive model of laser drilling of titanium is presented using different spatial laser intensity profiles. With the use of Comsol multiphysics®, deformation and cavity formation due to recoil pressure is modeled. It has been pointed out that gaussian intensity results in tapered shape cavity similar to keyhole, it also inherits poor finish due to adherence of molten material inside the keyhole wall. Whereas top hat intensity profile results in uniform shape cavity, however the size of pile up molten material near the edge of cavity increases with irradiation time.

The study is useful in optimizing the laser parameters prior to experiments to obtain features with minimum re-solidification, which in turn affect the surface roughness of the generated cavity.

6. References

1. Boyer, R. R. An overview on the use of titanium in the aerospace industry. *Materials Science and Engineering: A*, ***213*****(1)**, 103-114(1996).

2. Bruyere, V., Touvrey, C., Namy, P., A phase field approach to model laser power control in spot laser welding. *Proceedings of the 2014 COMSOL conference*, Cambridge (2014).

3. Zhang, Y., Shen, Z., Ni, X., Modeling and simulation on long pulse laser drilling processing. *International Journal of Heat and Mass Transfer*, **73**, 429-437 (2014).
4. Zhang, Y., Li, S, Chen, G., Mazumder, J., Experimental observation and simulation of keyhole dynamics during laser drilling. *Optics & Laser Technology* , **48**, 405-414 (2013).
5. Low, D.K.Y., Li, L., Byrd, P. J., Hydrodynamic physical modelling of laser drilling, *Journal of Manufacturing Science Engineering* , **124**, 852-862 (2002).
6. Ng, G.K.L., Crouse, P.L., Li, L., An analytical model for laser drilling incorporating effects of exothermic reaction, pulse width and hole geometry. *International Journal of Heat and Mass Transfer* , **49**, 1358-1374 (2006).
7. Anisimov, S. I., & Khokhlov, V. A. Instabilities in laser-matter interaction. CRC press. (1995)
8. Allmen, M., Blatter, A., Laser-Beam Interactions with materials, 2nd edition Springer, New York.
9. Yang et al., Experimental investigation and 3D finite element prediction of the heat affected zone during laser assisted machining of Ti6Al4V alloy, *Journal of Materials Processing Technology,* **210**, 2215-2222 (2010).
10. Rai, R., Burgardt, P., Milewski, J.O., Lienert, T. J., DebRoy, T., Heat transfer and fluid flow during electron beam welding of 21Cr-6Ni-9Mn steel and Ti-6Al-4V alloy, *Journal of Physics D:Applied Physics* , **42** (2009).
11. Zhang, Z., Modeling of Al evaporation and Marangoni flow in Electron Beam Button Melting of Ti6Al4V. *MASc Thesis, University of British Columbia* (2013).
12. Mills, K.C. Recommended values of thermophysical properties for selected commercial alloys, *Woodhead Publishing Ltd*., ISBN 978-1855735699, Cambridge (2002).
13. Lips, T., & Fritsche, B. A comparison of commonly used re-entry analysis tools. *Acta Astronautica*, ***57*****(2)**, 312-323 (2005).

7. Appendix

Table 1: Thermo-physical material properties

Thermo-physical properties	**Value**
Melting Temperature (K) [9]	1923
Thermal expansion coefficient (1/K) [10]	8e-6
Vaporization Temperature (K) [10]	3315
Density (kg/m^3) [11]	4200 (0-1923K) 3780 (1923-5000K)
Thermal Conductivity (W/(mK)) [11]	7.5(0K) 34.1(1923K) 37(3315K)
Specific heat(J/(kgK)) [11]	550(0K) 850(1923-5000K)
Latent heat of melting (J/kg) [12]	2.86e5
Latent heat of evaporation (J/kg) [12]	9.83e6
Temperature derivative of the surface tension (N/m*K) [12]	-0.28e-3
Dynamic viscosity(Pas)[12]	3.25e-3 (1923K) 3.03e-3 (1973K) 2.66e-3 (2073K) 2.36e-3 (2173K)
Universal gas constant (J/(kg*K))	8.314
Emissivity [13]	0.1536+1.8377e-4×(T-300K)